The *Drosophila* deoxyhypusine hydroxylase homologue *nero* and its target eIF5A are required for cell growth and the regulation of autophagy

Prajal H. Patel,[1,2] Mauro Costa-Mattioli,[3] Karen L. Schulze,[4] and Hugo J. Bellen[1,2,3,4]

[1]Program in Developmental Biology, [2]Department of Molecular and Human Genetics, [3]Department of Neuroscience, and [4]Howard Hughes Medical Institute, Baylor College of Medicine, Houston, TX 77030

Hypusination is a unique posttranslational modification by which lysine is transformed into the atypical amino acid hypusine. eIF5A (eukaryotic initiation factor 5A) is the only known protein to contain hypusine. In this study, we describe the identification and characterization of *nero*, the *Drosophila melanogaster* deoxyhypusine hydroxylase (DOHH) homologue. *nero* mutations affect cell and organ size, bromodeoxyuridine incorporation, and autophagy. Knockdown of the hypusination target *eIF5A* via RNA interference causes phenotypes similar to *nero* mutations. However, loss of *nero* appears to cause milder phenotypes than loss of *eIF5A*. This is partially explained through a potential compensatory mechanism by which *nero* mutant cells up-regulate eIF5A levels. The failure of eIF5A up-regulation to rescue *nero* mutant phenotypes suggests that hypusination is required for eIF5A function. Furthermore, expression of enzymatically impaired forms of DOHH fails to rescue *nero* clones, indicating that hypusination activity is important for *nero* function. Our data also indicate that *nero* and *eIF5A* are required for cell growth and affect autophagy and protein synthesis.

Introduction

Hypusination is a unique form of posttranslational modification occurring in eukaryotic organisms that transforms the amino acid lysine into the atypical amino acid hypusine (Park et al., 1982, 1997; Gordon et al., 1987). Thus far, a specific lysine residue on eIF5A (eukaryotic initiation factor 5A) is the only known target for this modification (Cooper et al., 1983; Smit-McBride et al., 1989). The formation of hypusine occurs via a two-step process. Each step of this process is catalyzed by a different enzyme (Park et al., 1982). In the first step, deoxyhypusine synthase (DHS) cleaves spermidine and transfers the 4-amino butyl moiety to a specific lysine residue of eIF5A (Wolff et al., 1990). In the second step, deoxyhypusine hydroxylase (DOHH) hydroxylates deoxyhypusine and irreversibly completes the hypusination process (Abbruzzese et al., 1986; Park et al., 2003). The protein responsible for DOHH function has only recently been identified and characterized. DOHH is an atypical hydroxylase consisting of eight HEAT (named after huntingtin, elongation factor 3, protein phosphatase 2A, and target of rapamycin [Tor]) repeat motifs (Joe et al., 1995; Kang et al., 1995; Park et al., 2006). DOHH is a metalloenzyme that requires iron ions for enzymatic activity (Park et al., 1982; Kim et al., 2006). Four conserved histidine–glutamic acid metal-binding motifs have been identified in DOHH (Park et al., 2006). Mutagenesis of these binding motifs impairs the enzyme's ability to bind iron and concomitantly abolishes its enzymatic activity (Kang et al., 2007).

Several lines of evidence suggest that eIF5A plays a role in cell proliferation. Inhibition of eIF5A function through drug-mediated hypusination blockage causes proliferation arrest in mammalian cell lines. Spermidine analogues that inhibit DHS activity as well as various metal ion chelators that inhibit DOHH enzymatic function have been shown to affect proliferation in vitro (Park et al., 1982, 1994; Jakus et al., 1993; Hanauske-Abel et al., 1994). Furthermore, inhibiting hypusination through cellular spermidine depletion also blocks cell proliferation in both mammalian cell lines as well as in yeast (Byers et al., 1994;

Correspondence to Hugo J. Bellen: hbellen@bcm.tmc.edu

Abbreviations used in this paper: APF, after puparium formation; DHS, deoxyhypusine synthase; Dlg, Discs large; DOHH, deoxyhypusine hydroxylase; dsRNA, double-stranded RNA; FLP, flippase; FRT, FLP recombination target; hDOHH, human DOHH; Su(H), suppressor of Hairless; Tor, target of rapamycin; UAS, upstream activation sequence.

The Rockefeller University Press $30.00
J. Cell Biol. Vol. 185 No. 7 1181–1194
www.jcb.org/cgi/doi/10.1083/jcb.200904161

Chattopadhyay et al., 2003). More direct evidence supporting a role for eIF5A in proliferation comes from genetic studies in yeast. Mutations in *TIF51A* and *TIF51B*, which encode eIF5A, or loss of *DYS1* (DHS homologue) in yeast cause cell inviability as well as G1–S phase arrest (Schnier et al., 1991; Wöhl et al., 1993; Sasaki et al., 1996; Park et al., 1998; Chatterjee et al., 2006). Interestingly, *LIA1* (*ligand of eIF5A 1*; yeast DOHH) is not essential for viability and has only a mild effect on the proliferative ability of *Saccharomyces cerevisiae* (Park et al., 2006). Moreover, the function of *LIA1* remains unknown as no major phenotypes are associated with its loss.

Lack of evidence supporting a role for yeast DOHH in eIF5A proliferation regulation questions the importance of the second step in the hypusination process. Thus, the only current evidence that argues for a role for DOHH in eIF5A regulation comes from drug studies that block DOHH enzymatic function through metal ion chelators in mammalian cell culture systems (Park et al., 1982; Hanauske-Abel et al., 1994), leading to the argument that the second step in the hypusination process is probably important only in higher eukaryotes. However, the effect of metal ion chelators on proliferation may be nonspecific. Therefore, genetic experiments on DOHH in higher eukaryotic organisms may shed light on the importance of the second step in the hypusination pathway.

This study addresses the function of DOHH in *Drosophila melanogaster*. Mutations in *nero*, the *Drosophila* DOHH homologue, were identified in a genetic screen for genes that regulate bristle number. *nero* is essential for organismal viability and plays a role in a wide number of important processes such as cell growth, proliferation, and autophagy. These phenotypes are reminiscent of mutations in the Tor pathway, but no clear epistatic relationship was found to exist between these pathways. As eIF5A is the sole known target of hypusination, we analyzed eIF5A function using RNAi. Loss of *eIF5A* causes phenotypes highly similar to but more severe than *nero*. The similarities in phenotypes imply that both *nero* and *eIF5A* govern the same processes. This also implicates *eIF5A* in processes besides proliferation, including autophagy and cell growth. Interestingly, we find that eIF5A is highly up-regulated in *nero* mutants. This up-regulation may partially compensate for the loss of *nero* and possibly accounts for the differences in the severity of the phenotypes of the loss of either gene. Furthermore, we find that the disruption of DOHH enzymatic activity impairs *nero* function, suggesting that its hypusination function is critical for its function. Finally, knockdown of either eIF5A or Nero through RNAi in S2 cells affects translation elongation.

Results

nero mutations in *Drosophila* DOHH affect sensory organ development

Lyman et al. (1996) performed a *P* element screen to identify insertions that alter bristle number in fruit flies and identified several insertions within genes previously implicated in bristle development. A similar screen in a genetically well-controlled background confirmed that such screens can be used for the purposes of identifying genes that govern neural development (Norga et al., 2003). One *P* element strain, $P[lArB]^{K48}$, which was generated in the initial Lyman et al. (1996) screen, exhibits a subtle bristle loss in homozygous flies. Therefore, we decided to focus on this *P* element insertion. $P[lArB]^{K48}$ is inserted in an intron of the *CG1910* gene and in close proximity to *CG2245*, potentially affecting both genes (Fig. 1 A). We identified a second *P* element, $P[lacW]^{s1921}$, associated with this locus and inserted within the 5′ untranslatable region of *CG2245* (Fig. 1 A; Spradling et al., 1999). We excised both $P[lArB]^{K48}$ and $P[lacW]^{s1921}$ and consequently generated three homozygous lethal mutations. To determine whether these mutations affect bristle development, each of the three mutant alleles was recombined onto a flippase (FLP) recombination target (FRT) chromosome for clonal analysis (Xu and Rubin, 1993). Mutant clones generated on the thorax show bristle loss as well as very small bristles (Fig. 1 B). Therefore, we named the gene *nero* after a nearly bald Flemish comic book character. Two mutations derived from $P[lacW]^{s1921}$, $nero^{1}$ and $nero^{2}$, are associated with small molecular deletions in *CG2245* that remove 189 bp and 123 bp, respectively, of the gene's open reading frame (Fig. 1 A). Animals carrying these mutations die as second instar (L2) larvae whether they are homozygous or in heteroallelic combinations (Fig. 1 E). Larvae carrying *nero* alleles in combination with a deficiency that spans the *CG2245* genomic region also die as second instar animals, suggesting that all *nero* alleles are strong loss of function alleles or null alleles (Fig. 1 E).

To verify that the *nero* mutations constitute a loss of *CG2245*, we generated a 1.5-kb genomic rescue construct containing the *CG2245* coding region (Fig. 1 A). This construct is sufficient to rescue the lethality of *nero* mutant larvae to full viability as well as bristle phenotypes associated with *nero* clones (Fig. 1 C). Ubiquitous overexpression of *CG2245* cDNA under upstream activation sequence (UAS) regulation using the *actin-GAL4* driver rescues the lethality associated with *nero* mutations (Brand and Perrimon, 1993). Furthermore, overexpression of *CG2245* in *nero* mutant clones using mosaic analysis with a repressible cell marker system is able to rescue the bristle phenotypes (Fig. 1 D; Lee and Luo, 1999). Altogether, these experiments demonstrate that *nero* mutations correspond to a loss of *CG2245*. Interestingly, *nero* overexpression in a wide variety of contexts using different *GAL4* drivers has no phenotypic effects.

CG2245 encodes a 302-aa protein bearing a high level of homology to eukaryotic DOHH proteins (57% identity with *Caenorhabditis elegans* and mouse homologues and a 59% identity with its human homologue). Thus, *nero* likely encodes the *Drosophila* DOHH homologue. Similar to the yeast and vertebrate homologues, the *Drosophila* DOHH protein consists of two dyads of four HEAT repeat domains (Fig. 1 F; Park et al., 2006). The human DOHH (hDOHH) protein bears four histidine–glutamic acid motifs important for DOHH enzymatic activity. These motifs are also conserved in the fly homologue, suggesting functional conservation.

Nero localizes to the ER

To determine the spatial expression of Nero as well as its subcellular localization, an antibody was raised against the full-length protein. The antibody specifically recognizes the Nero protein in immunohistochemical labeling, as all immunoreactivity is lost in

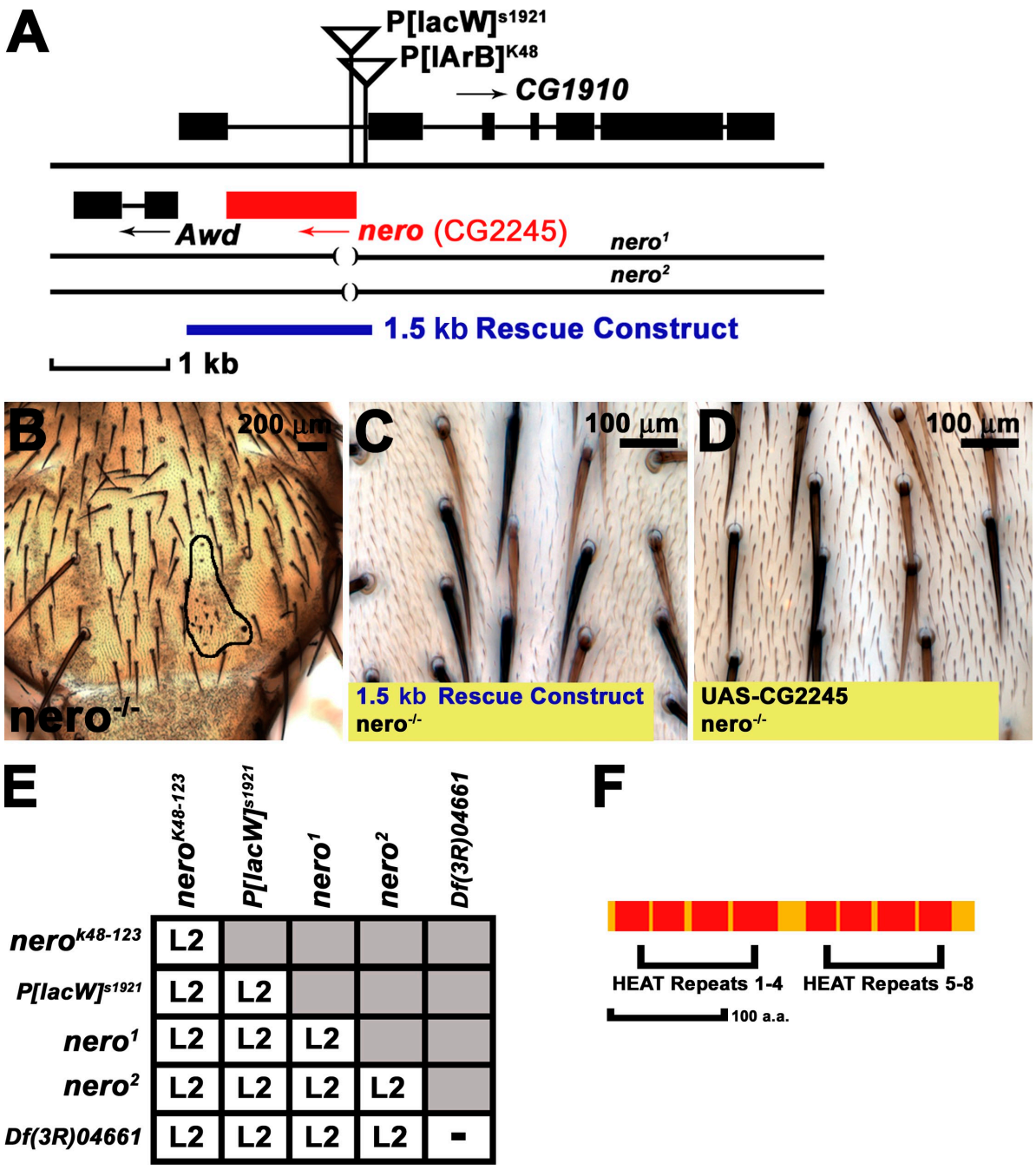

Figure 1. ***nero* mutants disrupt CG2245 and affect bristle size and viability.** (A) *nero* genomic locus. *P[lArB]*^{K48} and *P[lacW]*^{s1921} are both inserted within CG1910 and in proximity to CG2245 (shown in red). *nero*^{1} and *nero*^{2} alleles are derived from the excision of *P[lacW]*^{s1921} and disrupt the translational start of CG2245 (disrupted black lines). The 1.5-kb genomic rescue construct (shown in blue) rescues *nero* mutants to viability. (B) *nero* mutant clones (outlined in black) display a disruption in both the patterning and the size of bristles (genotype: *y w hs-FLP tub-GAL4 UAS-GFP-6xMYC-NLS/+; FRT82B nero*^{1}*/FRT82B hsp70-CD2 y*$^{+}$ *tub-GAL80*). (C) The 1.5-kb genomic rescue construct rescues bristle defects in *nero* mutant clones (genotype: *y w hs-FLP tub-GAL4 UAS-GFP-6xMYC-NLS/+; P[CaSper4–1.5 KB nero rescue]/+; FRT82B nero*^{1}*/FRT82B hsp70-CD2 y*$^{+}$ *tub-GAL80*). (D) Overexpression of the *nero* cDNA (CG2245) in *nero* mutant clones rescues bristle size defects (genotype: *y w hs-FLP tub-GAL4 UAS-GFP-6xMYC-NLS/+; UAS-nero/+; FRT82B nero*^{1}*/FRT82B hsp70-CD2 y*$^{+}$ *tub-GAL80*). (C and D) Rescued mutant bristles are marked by the recessive *yellow* mutation and appear light brown. (E) The lethal phase of *nero* mutants as homozygotes, in heteroallelic combinations, or in combination with *Df(3R)04661* is L2 lethal. (F) *nero* encodes a small 302-aa protein composed of two dyads consisting of four HEAT motifs each.

nero mutant clones (Fig. 2, A and B). This antibody also specifically recognizes Nero on Western blots as a single ~39-kD band in wild-type L2 protein lysates (Fig. 2 C). This band is not detected in *nero* mutant lysates. Thus, the ~39-kD band observed in wild-type lysates corresponds to the Nero protein (Fig. 2 C). The inability of the antibody to detect Nero in *nero* mutants is further evidence that the *nero* alleles are probably null alleles.

The Nero protein is expressed in larval imaginal disc cells (unpublished data). The subcellular distribution shows that the protein is excluded from the nucleus. The protein distribution

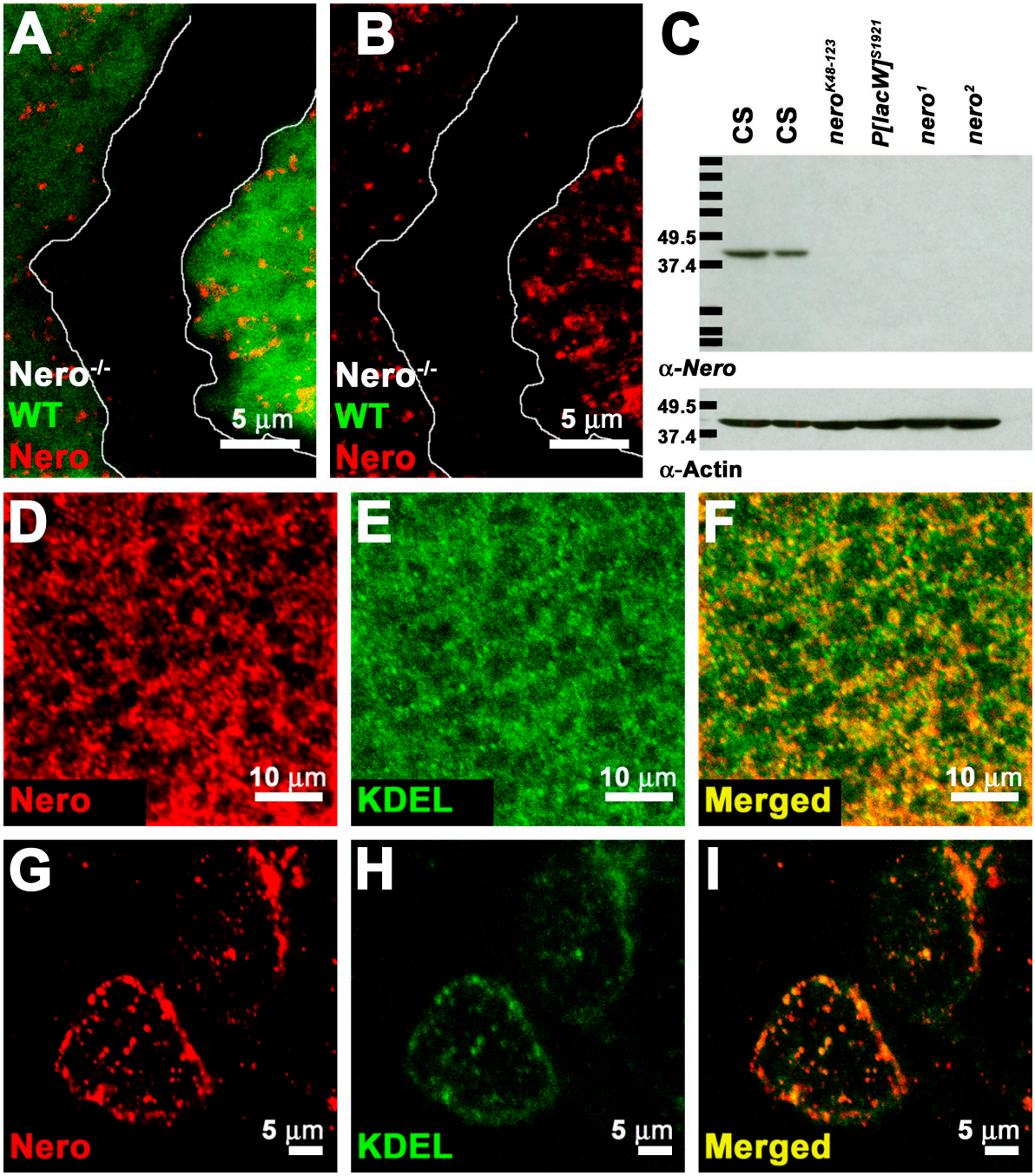

Figure 2. **Nero localizes to the ER.** (A–C) Antibodies generated against Nero specifically detect the Nero protein on both immunohistochemical preparations and Western blots. (A and B) Nero antibody fails to recognize the protein in mutant clones marked by the absence of GFP (genotype: *y w hs-FLP; FRT82B nero*^{1}*/FRT82B Ubi-GFP*). White lines mark the clonal boundary. WT, wild type. (C) The Nero antibody detects a single ∼39-kD band in *Canton-S* (CS) L2 larval protein extracts (first and second lanes) but fails to detect the protein in protein extracts from *nero*$^{k48\text{-}123}$ (third lane), *P[lacW]*^{s1921} (fourth lane), *nero*^{1} (fifth lane), and *nero*^{2} (sixth lane) L2 larvae on Western blots. Protein lysates from 10 larvae were loaded in each lane except the second lane, in which only five larvae were loaded. Actin was probed as a loading control. Protein standards run along with larval lysates are marked with black bars. Their sizes are recorded in kilodaltons on the left. (D–F) Double labeling of *Canton-S* third instar wing discs using the Nero antibody and the KDEL antibody shows extensive colocalization, demonstrating that Nero is ER associated. (G–I) Double labeling of *Canton-S* third instar garland cells using Nero and KDEL antibodies.

within the cell appears punctate, indicating that Nero is most likely associated with an organelle (Fig. 2 D). Double labeling of imaginal discs with the Nero antibody and a monoclonal antibody that recognizes the ER retention signal KDEL shows extensive colocalization, revealing that the Nero protein localizes at least in part to the ER (Fig. 2, D–F; Pelham, 1990). ER localization was also observed in larval garland cells (Fig. 2, G–I). As the Nero protein does not bear a signal peptide or a C-terminal KDEL sequence tag, Nero most likely associates with the external surface of the ER.

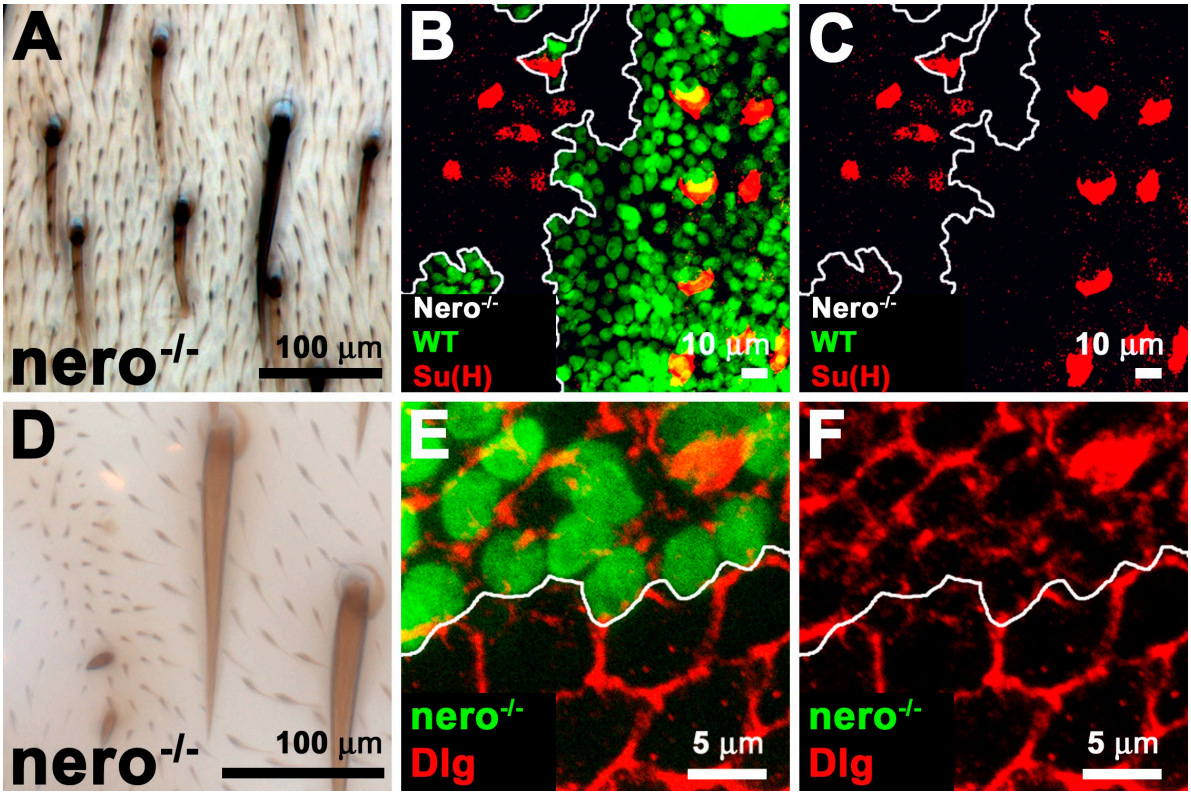

Figure 3. ***nero* is required for cell growth.** (A) The shaft and socket cells that comprise the external sensory organ on the thorax of the adult fly are typically shorter and smaller in *nero* mutant clones (genotype: *y w hs-FLP tub-GAL4 UAS-GFP-6xMYC-NLS/+; FRT82B nero*^{1}*/FRT82B hsp70-CD2 y*$^{+}$ *tub-Gal80*). Mutant bristles are marked by the recessive *yellow* mutation and appear light brown. (B and C) Socket cells observed 24 h APF labeled with Su(H) are smaller than wild-type (WT) socket cells (genotype: *y w hs-FLP/+; UAS-FLP/+; FRT82B nero*^{1}*/C684-GAL4 FRT82B Ubi-GFP M[3]*). The clone is marked by the absence of GFP. (D) Epidermal cells on the adult thorax in the vicinity of *nero* mutant bristles are often smaller in size, as indicated by smaller trichome size and closer trichome spacing (genotype: *y w hs-FLP/+; FRT82B nero*^{1}*/FRT82B Ubi-GFP*). (E and F) *nero* mutant epidermal cells in the thorax 47 h APF are smaller than adjacent wild-type cells. Thoraxes are labeled with Dlg to reveal cell outlines (genotype: *y w hs-FLP tub-GAL4 UAS-GFP-6xMYC-NLS/+; FRT82B nero*^{1}*/FRT82B hsp70-CD2 y*$^{+}$ *tub-GAL80*). The mutant clone is marked positively with GFP. (B, C, E, and F) White lines mark the clonal boundary.

nero is cell autonomously required for cell growth and affects the cell cycle

nero mutations cause both mild bristle loss as well as a severe reduction in bristle size (Figs. 1 B and 3 A). Bristles are composed of two external cells, the socket and the shaft. Socket cells dramatically increase in size within a 5-h period between the time points of their birth at 19 h after puparium formation (APF) and 24 h APF (Audibert et al., 2005). To determine whether the specification and the size of socket cells are affected early during the development of these cells, we labeled pupal thoraxes 24 h APF with the suppressor of Hairless (Su(H)) antibody, which is a marker for socket cells. Su(H) is expressed both in the cytoplasm and the nucleus of the socket cell, allowing visualization of the entire cell (Gho et al., 1996). As shown in Fig. 3 (B and C), *nero* mutant socket cells at this time point are much smaller than wild type. Thus, *nero* mutant socket cells are specified but fail to reach their mature size.

The growth defects observed in *nero* mutant clones are not specific to cells of the bristle lineage. As shown in Fig. 3 D, cells adjacent to *nero* mutant bristles are smaller in size as indicated by trichome size and spacing. This suggests that *nero* function is not confined solely to the regulation of bristle size. Indeed, ectodermal cells that lack *nero* in developing thoraxes 47 h APF are significantly smaller than adjacent wild-type cells (Fig. 3, E and F; Woods and Bryant, 1991). These defects are confined to *nero* mutant cells, and thus, *nero* is cell autonomously required for cell growth (Fig. 3, E and F). These *nero* mutant cells also show a decrease in Discs large (Dlg) expression, which is a basolateral cell membrane marker (Fig. 3, E and F). These effects on cell size are not restricted to the thorax, as rhabdomere size in mutant eye clones is also reduced when compared with adjacent wild-type cells, suggesting a defect in photoreceptor size (unpublished data). Thus, *nero* is cell autonomously required to achieve correct cell size in many tissues.

We further analyzed *nero* function by generating adult somatic clones using the *eyeless-FLP* system. *nero* mutant clones generated using the *eyeless-FLP* technique are generally irrecoverable (Fig. 4, A and B). Interestingly, *nero* mutant clones are easily obtained using *eyeless-FLP* when cell competition is ameliorated through the use of an FRT chromosome bearing a cell lethal mutation that effectively removes the mitotic wild-type, sister twin cells (Fig. 4 D). We observe similar results when competition is alleviated using a *Minute*. This suggests that *nero* mutant cells are viable but are at a competitive disadvantage. Indeed, *nero* mutant clones generated using this technique completely overtake the eye (Fig. 4, C and D). However, the resultant *nero* mutant eyes and heads are much smaller than wild-type heads and resemble the pinhead phenotype associated

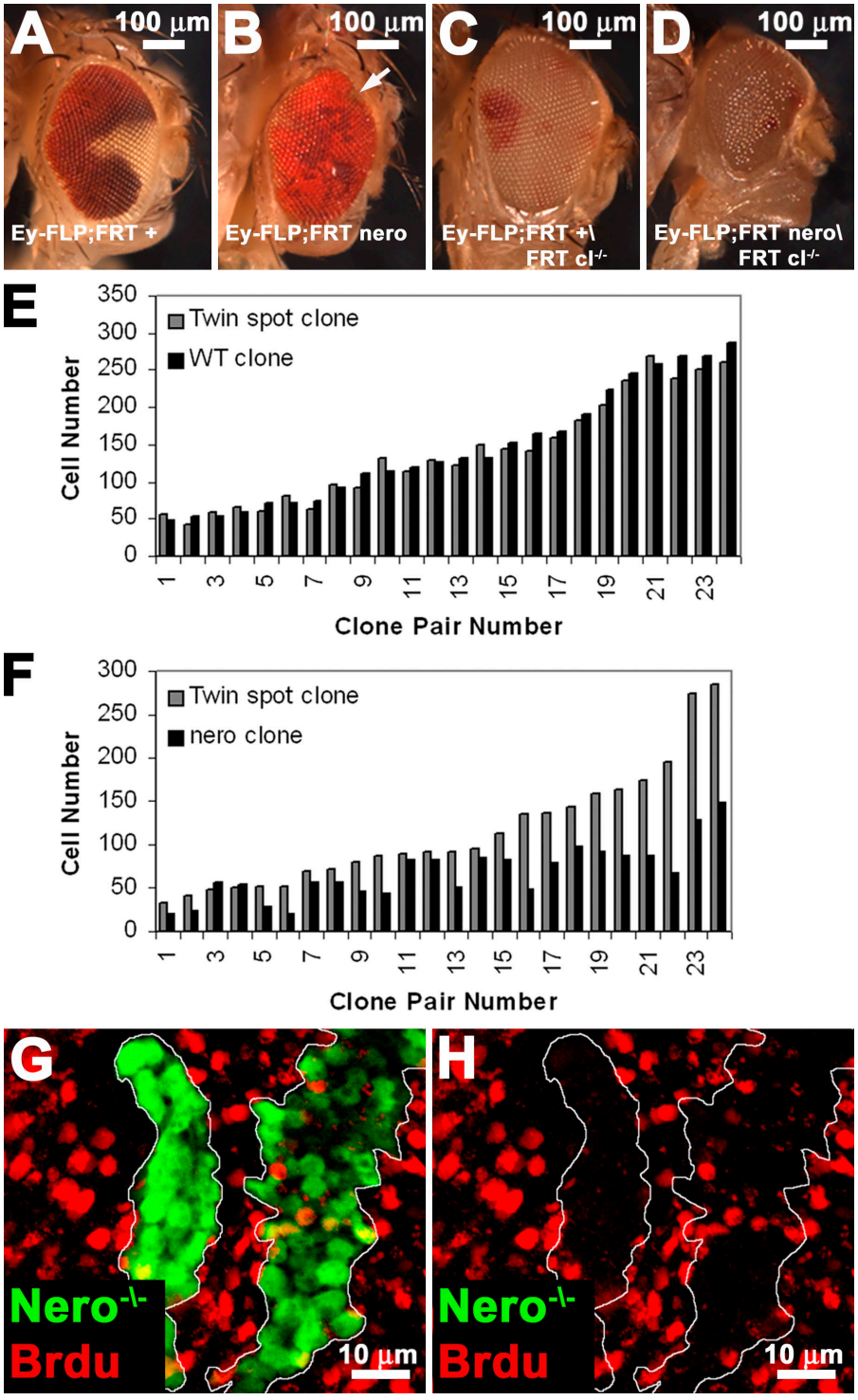

Figure 4. ***nero* regulates organ size, cell number, and proliferation.** (A and B) *nero* clones generated in a wild-type background are poorly competitive. Clones are marked with the absence of *white*$^+$ and thus appear white. (A) Wild-type clones are easily recovered (genotype: *y w eyeless-FLP GMR-lacZ/+; FRT82B+/FRT82B w*$^+$). (B) *nero* clones are usually irrecoverable (genotype: *y w eyeless-FLP GMR-lacZ/+; FRT82B nero*^{1}*/FRT82B w*$^+$). The white arrow points to a small *nero* mutant clone at the edge of the eye. (C and D) To provide *nero* mutant cells a competitive advantage, clones were made using an FRT-bearing chromosome carrying a recessive cell lethal that effectively eliminates wild-type twin spots. Clones are marked as in A and B. (C) Wild-type clones proliferate and take over most of the eye (genotype: *y w eyeless-FLP GMR-lacZ/+; FRT82B+/FRT82B w*$^+$ *l[3]cl*). (D) *nero* clones generated in a cell lethal background can, like wild type, dominate the entire eye (genotype: *y w eyeless-FLP GMR-lacZ/+; FRT82B nero*^{1}*/FRT82B w*$^+$ *l[3]cl*). *nero* mutant eyes and heads are smaller than wild-type control heads, suggesting a defect in organ size regulation. Eyes are also rough. (E) Cell number in wild-type (WT) clones is roughly similar to cell number in their twin spots (genotype: *y w hs-FLP; FRT82B +/FRT82B Ubi-GFP*). Black bars correspond to the clone, and gray bars correspond to the twin spot. (F) *nero* mutant clones have fewer cells than wild type (genotype: *y w hs-FLP; FRT82B nero*^{1}*/FRT82B Ubi-GFP*). Black and gray bars are the same as in E. (G and H) *nero* mutant clones marked positively with GFP incorporate BrdU more poorly than adjacent wild-type cells (genotype: *y w hs-FLP tub-GAL4 UAS-GFP-6xMYC-NLS/+; FRT82B nero*^{1}*/FRT82B hsp70-CD2 y*$^+$ *tub-GAL80*). White lines mark the clonal boundary.

with mutants in several growth pathways (Fig. 4 D; Oldham et al., 2000). Thus, *nero* mutations affect cell size and organ size, but *nero* is not required for cell viability.

Quantification of the number of cells in *nero* mutant clones versus the number of cells in their associated wild-type twin spot in the context of the wing imaginal disc reveals that *nero* mutant cells are underrepresented. Wild-type clones generated in the wing imaginal disc contain a similar number of cells when compared with the number of cells in their associated twin spot (Fig. 4 E). However, *nero* clones are smaller and contain fewer cells than their associated wild-type twin spots (Fig. 4 F). The differences in cell number between *nero* clones and their wild-type twin spots are less obvious in small clones and clearly increase as clones get larger (Fig. 4 F). This is likely caused by differences in Nero protein perdurance in small clones (Garcia-Bellido and Merriam, 1971). *nero* mutant cells are most likely eliminated because of an inability to compete with wild-type cells.

To determine whether the cell cycle is affected in *nero* mutant cells, we assayed their ability to incorporate BrdU (Gratzner, 1982). *nero* mutant clones show a decreased level of

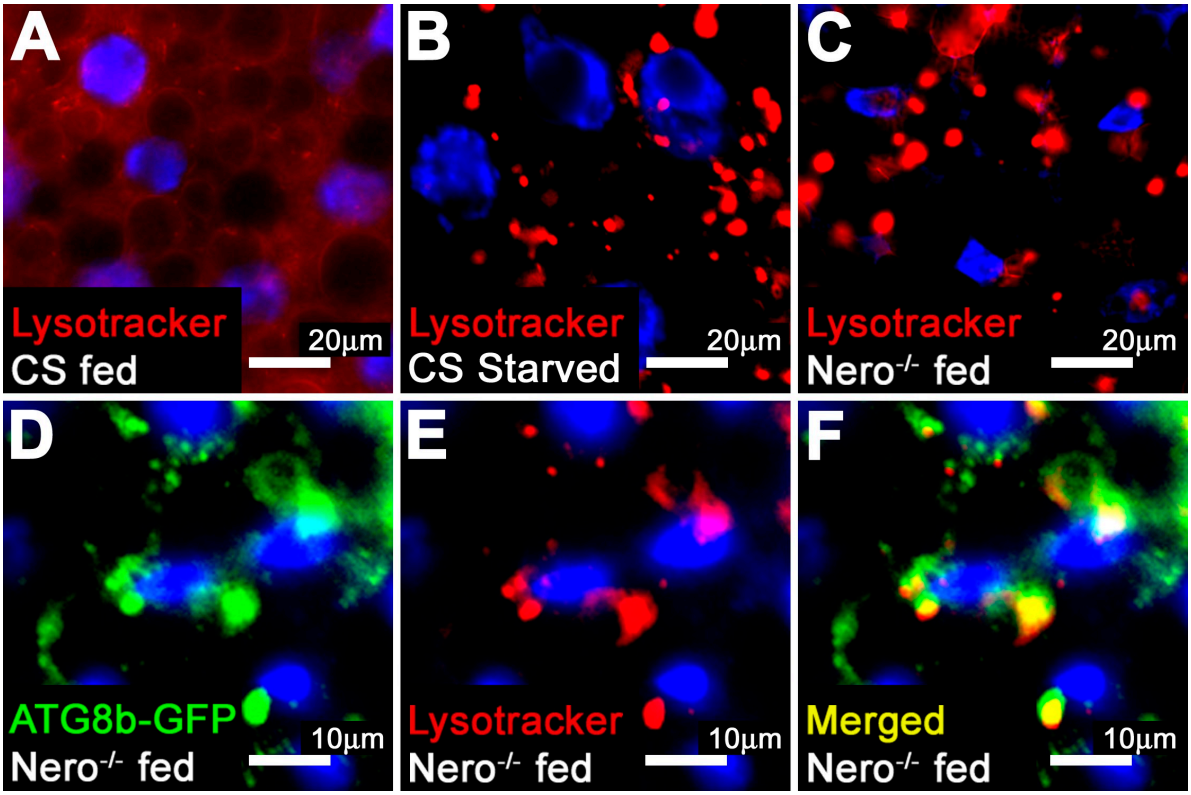

Figure 5. ***nero* mutants display autophagic starvation response.** (A) Fed second instar *Canton-S* (CS) larvae lack enlarged, acidic autophagic structures, as marked by LysoTracker fluorescence. (B) Second instar *Canton-S* animals subjected to a 4-h starvation period show LysoTracker-fluorescent autophagic structures. (C) Fed *nero*^{1} larvae display autophagic structures despite nutrient availability. (D–F) LysoTracker-fluorescent structures and ATG8b-GFP fusion proteins colocalize in *nero*^{1} mutant larvae, demonstrating that these structures are autophagosomes (genotype: *hs-ATG8b/+; FRT82B nero*^{1}*/FRT82B nero*^{1}).

BrdU incorporation, indicating a delay in cell cycle progression (Fig. 4, G and H). Thus, the data suggest that *nero* also plays a role in cellular proliferation.

nero negatively regulates autophagy

Several growth pathways like the Tor and insulin pathways are linked to the regulation of autophagy (Rusten et al., 2004; Scott et al., 2004). The induction of autophagy in the fat body is a cellular response to amino acid deprivation (Rusten et al., 2004; Scott et al., 2004). Larvae fed with an amino acid source lack autophagosomes in their fat bodies (Fig. 5 A; Rusten et al., 2004; Scott et al., 2004). However, upon amino acid withdrawal, enlarged, acidic intracellular structures are readily visible using the acidic pH reactive dye LysoTracker (Fig. 5 B; Rusten et al., 2004; Scott et al., 2004). These large structures have been shown to correspond to autophagosomes (Rusten et al., 2004; Scott et al., 2004). *nero* mutant larval fat bodies prominently display enlarged, acidified structures even when the animals are fed, suggesting that *nero* mutant larvae undergo a constitutive starvation response in the presence of an amino acid source (Fig. 5 C). To rule out a defect in feeding behavior, mutant larvae were fed yeast paste containing food dyes. *nero* mutant larvae feed properly, as animals show ample consumption of yeast paste (unpublished data).

To demonstrate that the acidified structures observed in *nero* mutant fat bodies are autophagosomes, ATG8b (autophagy-specific gene 8b)-GFP fusion proteins were overexpressed in *nero* mutants. ATG8b-GFP fusion proteins have been shown to localize to autophagic structures (Scott et al., 2004). LysoTracker-positive structures observed in *nero* mutant fat body cells co-localize with the ATG8b-GFP fusion proteins, confirming that these structures are indeed autophagosomes (Fig. 5, D–F).

The combination of defects in cell size and autophagy suggests a possible link between *nero* and the Tor pathway (Oldham et al., 2000; Zhang et al., 2000; Rusten et al., 2004; Scott et al., 2004). *Tsc1* (*tuberous sclerosis 1*) mutations cause constitutive activation of the Tor pathway and have the opposite phenotype of *nero* mutations. *Tsc1* mutations increase cell size, cause tissue overgrowth, increase cell number in clones when compared with their twin spot, and block the induction of autophagy (Gao and Pan, 2001; Potter et al., 2001; Tapon et al., 2001; Rusten et al., 2004; Scott et al., 2004). Therefore, we generated a *Tsc1 nero* double mutant chromosome to ascertain the possibility of an epistatic relationship between these genes. Unlike either *nero* or *Tsc1* clones, *Tsc1 nero* double mutant clones cannot be recovered (Fig. S1). Thus, *nero* and *Tsc1* do not exist in a straightforward epistatic relationship. Interestingly, *Tsc1* fully suppresses the autophagic defect seen in *nero* mutant animals (Fig. S1). However, this epistatic relationship is reversed in other contexts such as larval growth and developmental timing. *Tsc1* mutant larvae appear to undergo precocious development. We find that this precocious development is suppressed in the *Tsc1 nero* double mutant larvae (Fig. S1).

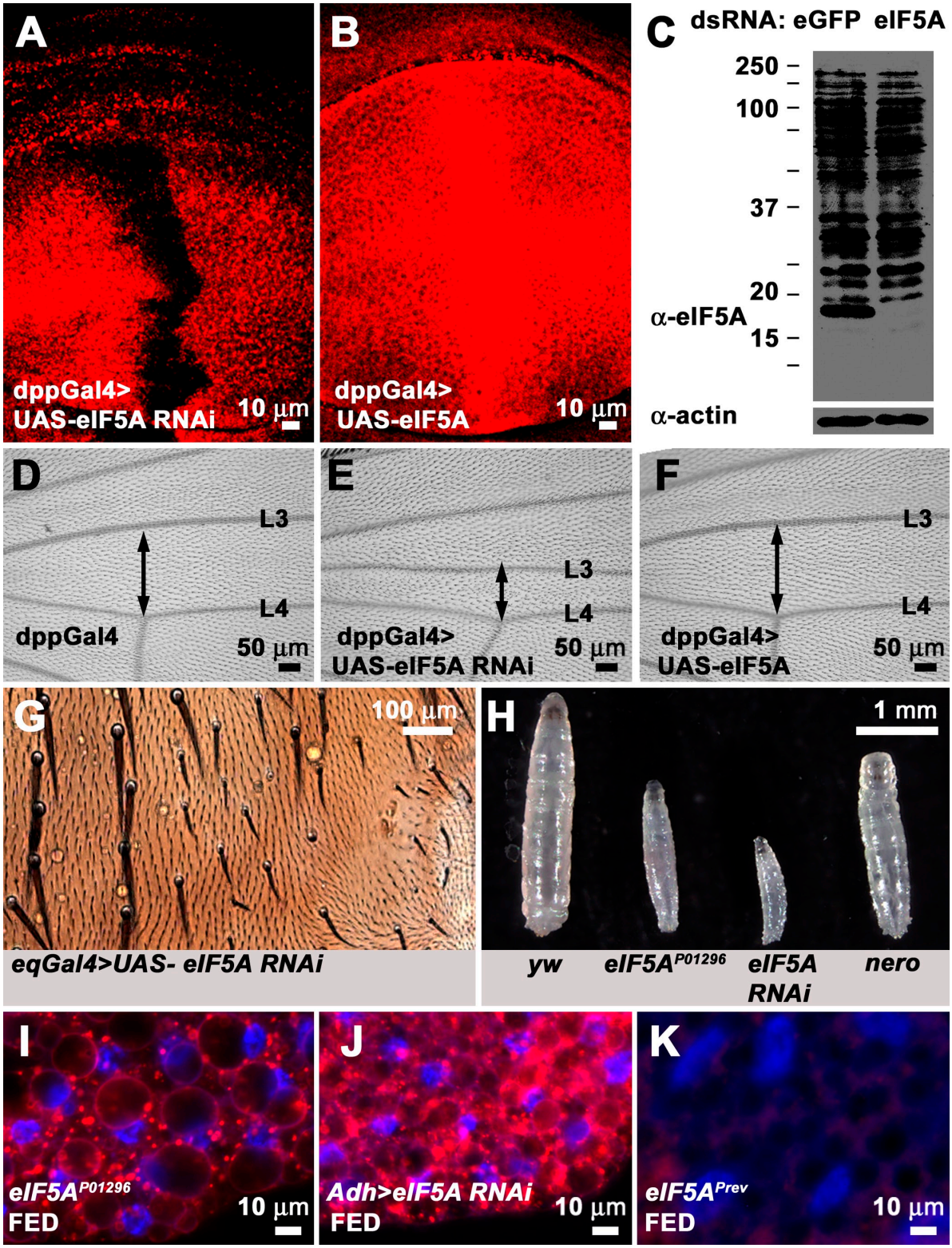

Figure 6. **Loss of eIF5A causes phenotypes reminiscent of *nero*.** (A) Wing imaginal disc in which *eIF5A* dsRNA has been expressed under the regulation of the *dpp-GAL4* driver line and labeled with anti-eIF5A antibody. Anti-eIF5A antibody fails to detect the eIF5A protein in cells expressing eIF5A dsRNA. (B) Wing imaginal disc in which *eIF5A* under UAS regulation has been overexpressed using *dpp-GAL4* and stained with anti-eIF5A antibody. Anti-eIF5A antibody detects the overexpressed eIF5A protein. (C) Anti-eIF5A antibody detects an ~17-kD band in EGFP dsRNA–treated S2 cells but fails to detect this band in eIF5A dsRNA–treated S2 cells. Actin is used as the loading control. Protein standards run along with S2 cell lysates are marked with black bars. Their sizes are recorded in kilodaltons on the left. (D) Control adult wing (genotype: *dpp-GAL/+*). (E) Adult wing in which *eIF5A* dsRNA has been expressed under the regulation of the *dpp-Gal4* driver. The distance between the L3 and L4 vein (double-headed arrow) is drastically reduced (genotype: *dpp-Gal4/UAS-eIF5A RNAi*). (F) Adult wing in which wild-type *eIF5A* under UAS regulation was overexpressed using *dpp-Gal4*. The distance between the L3 and L4 vein (double-headed arrow) appears similar to the experimental control (D; genotype: *dpp-GAL4/UAS-eIF5A RNAi*). (G) RNAi knockdown of

These results suggest that *nero* may not play a direct role in Tor signaling and most likely alters cell growth through an independent mechanism.

nero regulates eIF5A

eIF5A is generally believed to be the sole protein that undergoes hypusination in eukaryotic organisms (Cooper et al., 1983; Smit-McBride et al., 1989). Having established a genetic model in which loss of the second step of the hypusination process causes severe phenotypes, we decided to ascertain whether loss of eIF5A causes phenotypes similar to loss of *nero*, as would be predicted if *nero* regulated eIF5A function. To test this, we obtained an RNAi line purported to knock down eIF5A (Dietzl et al., 2007). We used a monoclonal antibody raised against the human eIF5A protein to test whether this RNAi line is able to effectively down-regulate eIF5A. Expression of *eIF5A* double-stranded RNA (dsRNA) under the regulation of *dpp-GAL4* strongly reduces the expression of eIF5A in a central stripe that runs down the middle of the wing imaginal disc, proving that the RNAi line is effective and that the antibody is able to specifically recognize the *Drosophila* eIF5A protein in vivo (Fig. 6 A). Additionally, this antibody is able to recognize the wild-type overexpressed eIF5A protein (Fig. 6 B). Unfortunately, it is difficult to detect the eIF5A protein on Western blots of larval lysates using this antibody. However, it recognizes an ~17-kD band on Western blots of S2 cell lysates, which corresponds to the expected molecular mass of eIF5A (Fig. 6 C). Furthermore, this 17-kD band is lost in S2 cell lysates treated with eIF5A dsRNA, suggesting that the band specifically corresponds to eIF5A (Fig. 6 C). Altogether, these data suggest that we can efficiently knock down or overexpress eIF5A using *UAS-eIF5A RNAi* or *UAS-eIF5A* constructs, respectively. We used *UAS-eIF5A RNAi* to test whether loss of eIF5A has any phenotypic consequences. Knockdown of eIF5A in the *dpp-GAL4* expression domain causes a narrowing of the region between the L3 and L4 wing veins, a phenotype which is often associated with growth mutants in *Drosophila* (Fig. 6, D and E). However, overexpression of eIF5A appears to have no phenotypic effect on the distance between L3 and L4 veins, and thus, like *nero*, overexpression of *eIF5A* has no overt phenotypic consequences (Fig. 6, D and F).

We decided to test whether loss of eIF5A causes phenotypes similar to those associated with *nero*. Flies carrying a transgenic *UAS-eIF5A RNAi* construct were crossed to the thoracic driver *eq-GAL4* to determine whether loss of eIF5A affects bristle size (Pi et al., 2001; Dietzl et al., 2007). We find that eIF5A knockdown results in decreased bristle size on the thorax, which is similar to what we observe in *nero* mutant clones (compare Fig. 6 G with Fig. 1 B). We also identified a homozygous lethal *P* element, $P[PZ]^{01296}$ ($eIF5A^{P01296}$), inserted within the first intron of *eIF5A* (Spradling et al., 1999). Excision of this *P* element reverts the lethality, indicating that the lethality is caused by the insertion. Homozygous mutant $eIF5A^{P01296}$ larvae exhibit a severe larval growth defect and are much smaller than wild-type larvae, although they live for 8 d (Fig. 6 H). RNAi knockdown of *eIF5A* using the ubiquitous driver *tub-GAL4* severely affects larval growth, and the effect is greater than the phenotype observed in $eIF5A^{P01296}$ larvae, suggesting that loss of eIF5A using RNAi perhaps constitutes a stronger loss of function condition than $eIF5A^{P01296}$ (Fig. 6 H). Thus, $eIF5A^{P01296}$ is most likely a hypomorphic mutation. Interestingly, *eIF5A* mutations are more severe than *nero* in terms of larval growth (Fig. 6 H). Finally, we find that the $eIF5A^{P01296}$ mutation also affects autophagy induction. Similar to *nero*, *eIF5A* mutant larval fat bodies undergo constitutive autophagy under fed conditions (Fig. 6 I). The autophagy defect is specific to the *P* element insertion, as the revertants do not show a defect in autophagy induction (Fig. 6 K). Driving *eIF5A* RNAi in larval fat bodies using *Adh-GAL4* likewise induces autophagy (Fig. 6 J). Thus, the phenotypes associated with loss of *eIF5A* are very similar to the phenotypes associated with loss of *nero*, suggesting that Nero and eIF5A function in the same pathway in flies.

If the target of *nero* function is eIF5A, loss of *eIF5A* ought to be epistatic to *nero*. Thus, *eIF5A; nero* double mutant larvae should resemble *eIF5A* mutant larvae. We find that *eIF5A; nero* double mutant larvae display a slightly more severe larval growth defect than *eIF5A* mutants alone (Fig. 7 A). As $eIF5A^{P01296}$ is probably not a null allele, the more severe phenotype is presumably a consequence of increased inactivation of residual eIF5A function in these animals.

Interestingly, the larval growth defect caused by the loss of *eIF5A* is more severe than loss of *nero* (Figs. 6 H and 7 A). This may be the result of several causes. One possibility is that eIF5A has both hypusination-dependent and -independent functions. Another possibility is that *nero* is required only for optimal *eIF5A* function, and thus, eIF5A maintains some modicum of activity in *nero* mutants. If eIF5A is still partially active even in the absence of hypusination, overexpression of *eIF5A* ought to ameliorate *nero* mutant phenotypes. To test this, we overexpressed *eIF5A* in *nero* mutant clones. We found that overexpression of *eIF5A* is not sufficient to rescue bristle size defects associated with *nero* mutant clones (Fig. 7 B). Moreover, we were surprised to find that eIF5A is strongly up-regulated in *nero* mutant clones (Fig. 7, C and D). This strong up-regulation possibly accounts for the weaker phenotype observed in *nero* mutant clones and may represent an adaptive response of the cells to the inefficiently functioning eIF5A protein.

Finally, to directly assess the requirement for DOHH activity, we overexpressed wild-type and enzymatically inactive versions of hDOHH in *nero* mutant clones. Alanine replacement of histidines 56, 89, 207, and 240 of hDOHH, all of which are conserved in the *Drosophila* protein, has been shown to abolish hypusine enzymatic function and iron-binding ability without affecting eIF5A substrate binding (Kang et al., 2007). These residues were mutated separately

eIF5A using *eq-GAL4* causes defects in bristle growth similar to *nero* mutations (genotype: *eq-GAL4/+; UAS-eIF5A RNAi*). (H) Synchronized larvae 72 h after egg hatching of four different genotypes (from left to right): *y w*, $eIF5A^{P01296}$, *tub-GAL4/UAS-eIF5A RNAi*, and $nero^{1}$. (I) $eIF5A^{P01296}$ larval fat bodies undergo constitutive autophagy under fed conditions. (J) RNAi knockdown of *eIF5A* in the fat body induces constitutive autophagy under fed conditions (genotype: *Adh-GAL4/+; UAS-eIF5A RNAi/+*). (K) Larval fat bodies of *P* element revertant $eIF5A^{Prev}$ do not undergo autophagy under fed conditions.

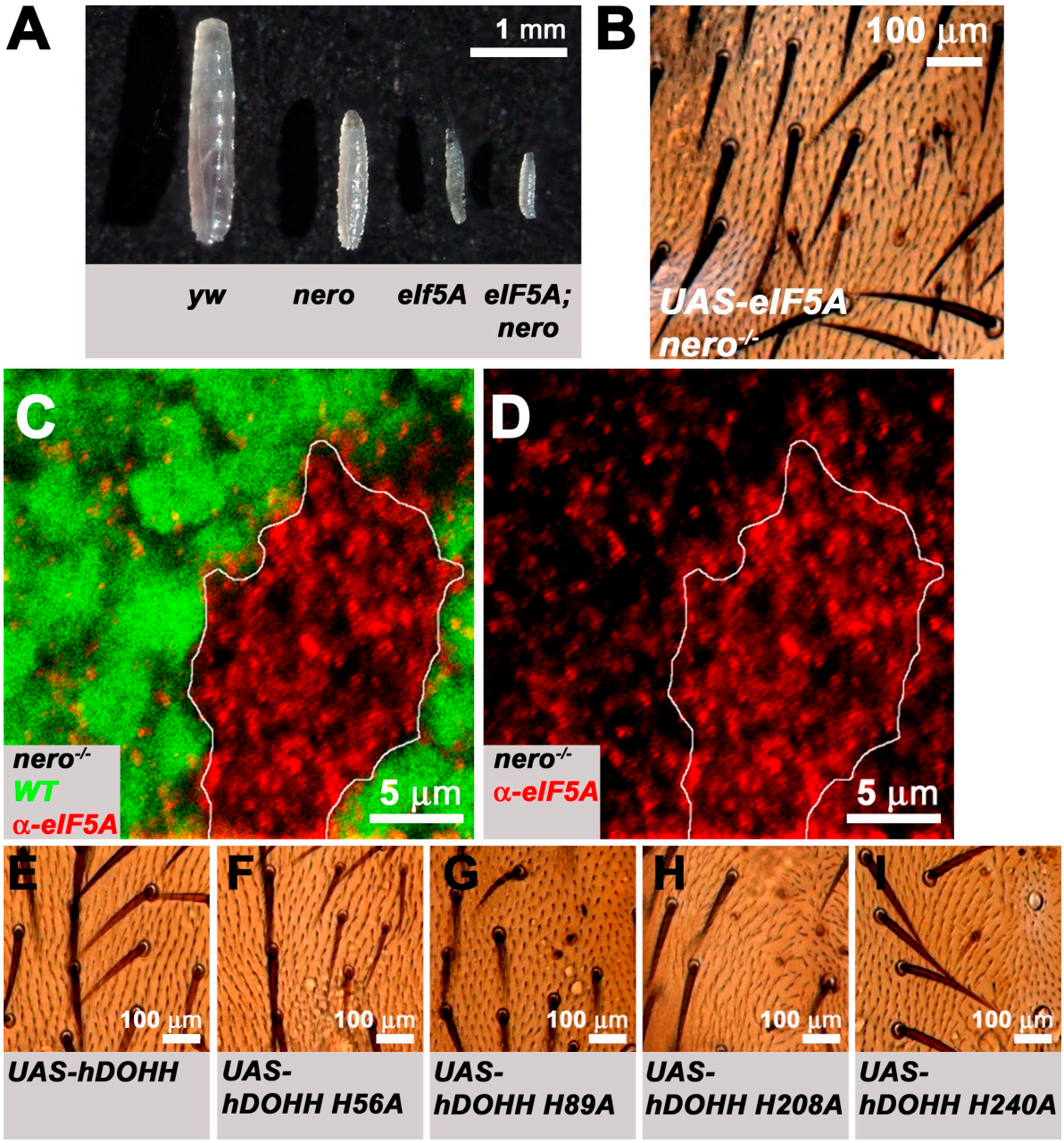

Figure 7. ***nero* regulates eIF5A levels in vivo and Nero's DOHH activity is required for *nero* function.** (A) Synchronized larvae 72 h after egg hatching of four different genotypes (from left to right): *y w*, *nero*^{1}, *eIF5A*^{P01296}, and *eIF5A*^{P01296}*; nero*^{1}. The growth of *eIF5A*^{P01296}*; nero*^{1} double mutant larvae appears to be more impaired than either *eIF5A*^{P01296} or *nero*^{1} homozygous mutant larvae. (B) Overexpression of eIF5A in *nero* mutant clones fails to rescue bristle growth defects associated with *nero* mutant clones (genotype: *y w hs-FLP tub-GAL4 UAS-GFP-6xMYC-NLS/+; UAS-eIF5A/+; FRT82B nero*^{1}*/FRT82B hsp70-CD2 y*$^{+}$ *tub-GAL80*). (C and D) eIF5A levels are dramatically up-regulated in *nero* mutant clones in the wing imaginal disc. *nero* mutant clones are marked by the absence of GFP (green; genotype: *y w hs-FLP; FRT82B nero*^{1}*/FRT82B Ubi-GFP*). White lines mark the clonal boundary. WT, wild type. (E) Overexpression of hDOHH in *nero* mutant clones rescues bristle size defects (genotype: *y w hs-FLP tub-GAL4 UAS-GFP-6xMYC-NLS/+; UAS-hDOHH/+; FRT82B nero*^{1}*/FRT82B hsp70-CD2 y*$^{+}$ *tub-GAL80*). (F–I) Overexpression of mutated forms of hDOHH in *nero* mutant clones fails to rescue bristle size defects. Genotypes are essentially identical to E except mutated forms of hDOHH are expressed under the *UAS* regulation. (F) Genotype: *y w hs-FLP tub-GAL4 UAS-GFP-6xMYC-NLS/+; UAS-DOHH H56A/+; FRT82B nero*^{1}*/FRT82B hsp70-CD2 y*$^{+}$ *tub-GAL80*. (G) Genotype: *y w hs-FLP tub-GAL4 UAS-GFP-6xMYC-NLS/+; UAS-hDOHH H89A/+; FRT82B nero*^{1}*/FRT82B hsp70-CD2 y*$^{+}$ *tub-GAL80*. (H) Genotype: *y w hs-FLP tub-GAL4 UAS-GFP-6xMYC-NLS/+; UAS-hDOHH H208A/+; FRT82B nero*^{1}*/FRT82B hsp70-CD2 y*$^{+}$ *tub-GAL80*. (I) Genotype: *y w hs-FLP tub-GAL4 UAS-GFP-6xMYC-NLS/+; UAS-hDOHH H240A/+; FRT82B nero*^{1}*/FRT82B hsp70-CD2 y*$^{+}$ *tub-GAL80*. (B and E–I) Mutant bristles are marked by the recessive *yellow* mutation and appear light brown.

in the hDOHH cDNA and introduced into flies to determine whether these proteins could complement the loss of *nero*. Overexpression of the wild-type hDOHH protein fully complements defects in bristle size associated with *nero* mutant clones on the thorax and does not cause any other obvious phenotype (Fig. 7 E). This result demonstrates that *nero* is the DOHH homologue in flies. However, overexpression of the four different enzymatically inactive mutant proteins in *nero* mutant clones fails to rescue defects in bristle size, revealing the importance of the hypusination activity for *nero* function (Fig. 7, F–I).

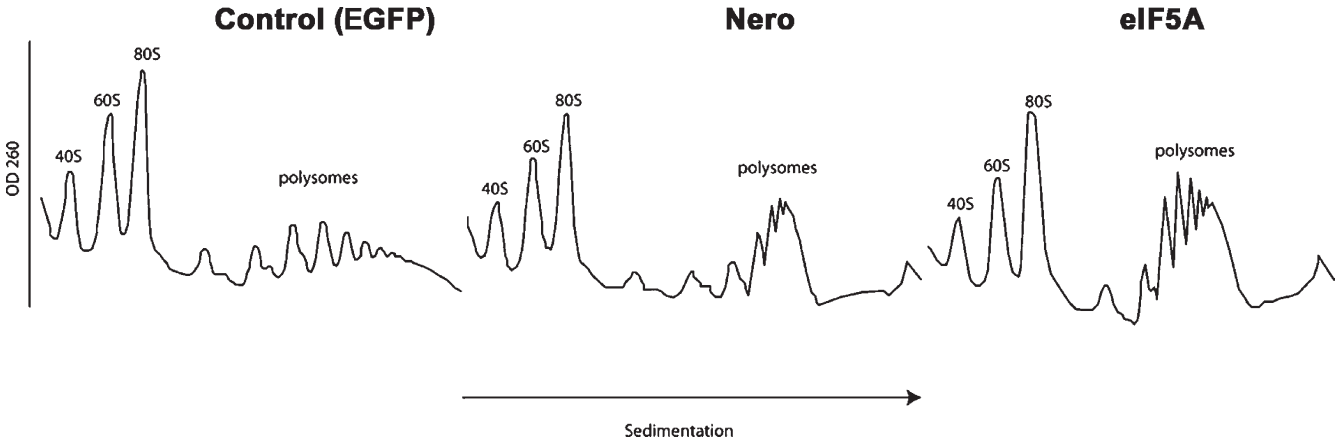

Figure 8. **RNA knockdown of either Nero or eIF5A blocks translation elongation in *Drosophila* S2 cells.** Polysome analysis of *EGFP*, *nero*, and *eIF5A* dsRNA–treated S2 cells. Cells were harvested, lysed, and fractionated by centrifugation on a 10–50% sucrose gradient. Polysomes were analyzed as described in Materials and methods. *EGFP* (left), *nero* (middle), and *eIF5A* dsRNA–treated (right) images are shown. The positions of the polysomes and ribosomes are indicated.

Both Nero and eIF5A regulate protein synthesis

Recent evidence supports the idea that eIF5A regulates translation elongation. Gregio et al. (2009) have shown that the polysome (number of ribosomes per mRNA) profile of a yeast eIF5A mutant resembles that of a translation elongation mutant.

As eIF5A is thought to be the only target for Nero, we predicted that reduction of either Nero or eIF5A should have a similar effect on protein synthesis. To test this hypothesis, we used polysome profiling. Polysome sedimentation in sucrose gradients is one of the most powerful techniques for studying translational control. In this technique, the mRNAs are separated by ultracentrifugation as a function of the number of ribosomes to which they are associated. Conditions that reduce translation elongation result in the binding of mRNAs to multiple ribosomes, thus causing an increase in sedimentation toward the polysomal fraction. We established conditions to decrease levels of either Nero or eIF5A using dsRNA in *Drosophila* S2 cells (unpublished data). Similar to the yeast *eIF5A* mutant, RNAi-mediated knockdown of either Nero or eIF5A increases polysome size, indicating a defect in translation elongation (Fig. 8; Gregio et al., 2009). These data suggest that Nero-mediated eIF5A hypusination regulates translation rates.

Discussion

Hypusination, the transformation of the amino acid lysine into the atypical amino acid hypusine, is a process that has been documented in numerous eukaryotic organisms from yeast to humans (Park et al., 1982, 1997; Gordon et al., 1987). The precise function of eIF5A and the significance of hypusination with regard to eIF5A function remain obscure. This study presents the functional characterization of the *Drosophila* DOHH homologue *nero* and looks at *nero* function in relation to eIF5A.

nero is an essential gene and encodes a highly conserved homologue of hDOHH

nero is required for organismal viability in *Drosophila*. This is in stark contrast to yeast, in which yeast DOHH (*LIA1*) is not an essential gene (Park et al., 2006). This has lead to the hypothesis that the second step in the hypusination process may not be essential in regard to eIF5A function in lower eukaryotes (Park et al., 2006). We find that DOHH activity is important in higher eukaryotes. The generation of null mutations of *nero* and the rescue of these mutants using the *Drosophila* DOHH cDNA/genomic rescue constructs formally confirm that DOHH function is required in higher eukaryotic organisms such as *Drosophila*.

The Nero protein appears to be highly conserved in *Drosophila*. Nero shares 59% amino acid identity with its hDOHH homologue, and the hDOHH protein can substitute for the *Drosophila* protein in vivo. Overexpression of hDOHH in *nero* mutant clones is able to fully rescue the short bristle defect observed in *nero* mutant clones. Thus, *nero* constitutes a true homologue of hDOHH. Analysis of hDOHH function has shown that DOHH is a metalloenzyme that requires iron ions for enzymatic activity (Park et al., 1982; Kim et al., 2006). Four histidine–glutamic acid metal-binding motifs have been identified in hDOHH, and these motifs have been shown to be required for DOHH enzymatic function (Park et al., 2006; Kang et al., 2007). These four motifs are fully conserved in the *Drosophila* homologue. Interestingly, overexpression of hDOHH carrying mutations in these metal ion–binding motifs fails to complement *nero* mutations, arguing that these residues are also important for DOHH function in *Drosophila*. All together, Nero appears to be highly conserved both in terms of amino acid homology as well as important residues critical for its function.

nero is required for cell growth, protein synthesis, and autophagy regulation

Clonal analyses of *nero* mutations during imaginal disc development implicate *nero* in cell growth. Loss of *nero* causes small bristles, epidermal cells, and photoreceptors. Furthermore, removing *nero* function in the developing *Drosophila* eye-antennal disc causes decreased head size, suggesting that *nero* function is required for organ size. Mutations that negatively affect cell growth share an array of common phenotypes such as impaired cell competitive ability and altered cell cycle.

Such combined defects in cell growth, impaired competitive ability, and altered cell cycle are often attributed to impaired or reduced translation (Neufeld et al., 1998; Moreno et al., 2002). We find that loss of *nero* also affects both competitive ability and altered cell cycle phasing, as indicated by the fact that *nero* mutant cells are poorly recovered and that they poorly incorporate BrdU. All together, these phenotypes suggest that *nero* plays a role in the regulation of translation.

Consistent with the notion that Nero regulates eIF5A activity, inhibition of Nero or eIF5A by RNAi causes a similar impairment in translation elongation. This finding is consistent with data generated in other experimental systems. eIF5A has been shown to bind to components of the translational machinery in a hypusine-dependent manner (Zanelli et al., 2006). Furthermore, depletion of yeast eIF5A has been shown to block protein synthesis as well as alter polysome profiles (Kang and Hershey, 1994; Gregio et al., 2009). Our data support a function for DOHH in eIF5A-mediated translational control.

Interestingly, *nero* also regulates the induction of autophagy. Unlike effects on translation, defects in the induction of autophagy are generally not common to all cell growth pathways. In *Drosophila*, defects in autophagy regulation have been associated with mutations that affect the insulin and Tor growth signaling pathways (Rusten et al., 2004; Scott et al., 2004). Amino acid nutrient availability has been proposed as an upstream regulator of Tor activity (Dann and Thomas, 2006). This is in line with the observation that starvation induces autophagy in *Drosophila* (Rusten et al., 2004; Scott et al., 2004). This prompted us to test *nero* for a potential role in the Tor pathway. However, we were unable to generate any conclusive genetic evidence to link the two pathways, allowing us to exclude at the very least an integral role for *nero* in the Tor growth pathway.

Phenotypes associated with loss of eIF5A resemble *nero*, and *nero* regulates eIF5A levels

Inhibition of eIF5A using RNAi-mediated knockdown causes phenotypes similar to the ones observed in *nero* mutants. Knockdown of eIF5A, the target of hypusination, recapitulates *nero* mutant phenotypes, including decreased bristle size, autophagy, and defects in larval growth/development. These observations suggest that both *nero* and *eIF5A* regulate similar processes in vivo and argue that *nero* is linked to eIF5A function.

Interestingly, we find that eIF5A is up-regulated in *nero* mutants. This effect on eIF5A levels in DOHH mutants has not previously been reported. It is likely that the up-regulation of eIF5A constitutes an adaptive response by the cell to the loss of *nero*. Because the *eIF5A* mutant phenotype appears to be more severe than the defect observed in *nero* mutant animals, the up-regulation of eIF5A in *nero* mutants may explain the observed differences in larval growth associated with *eIF5A* and *nero* double mutants. Thus, incompletely hypusinated forms of eIF5A may still be partially functional and able to mildly ameliorate the *nero* mutant phenotype. This model is also compatible with the idea that the loss of *nero* causes only a partial loss of eIF5A activity. In conclusion, our work highlights the importance of *nero*/DOHH function in *Drosophila*, implicates *eIF5A* and *nero* in cell growth and autophagy regulation, and provides genetic evidence that links eIF5A function with *nero*/DOHH regulation.

Materials and methods

Drosophila stocks and genetics

We used the following stocks: *y w* (control), *Canton-S* (control), *P[lArB]^{K48}* (provided by T.F. MacKay, North Carolina State University, Raleigh, NC; Lyman et al., 1996), *FRT82B Tsc1^{Q87X}* (provided by P.H. Patel [Fred Hutchinson Cancer Research Center, Seattle, WA] and F. Tamanoi, [University of California, Los Angeles, Los Angeles, CA]; Tapon et al., 2001), *hs-ATG8b-GFP* (provided by T.P. Neufeld, University of Minnesota, Minneapolis, MN; Scott et al., 2004), *eq-GAL4* (Pi et al., 2001), *UAS-CG3186 RNAi* (Dietzl et al., 2007), *Adh-GAL4/CyO* (Fischer et al., 1988), *Ubx-FLP; FRT82B Ubi-GFP M(3), y w hs-FLP tub-GAL4 UAS-GFP-6xMYC-NLS; FRT82B hsp70-CD2 y$^+$ tub-GAL80/TM6* (provided by G. Struhl, Columbia University, New York, NY), *y w; D/TM3 Kr-GAL4 UAS-GFP*, and *FRT82B Ubi-GFP* (provided by G. Halder, The University of Texas M.D. Anderson Cancer Center, Houston, TX). *y w; Act-GAL4/CyO, Df(3R)04661, y w eyeless-FLP GMR-lacZ; FRT82B w$^+$ l(3)cl, FRT82B w$^+$, P[PZ]^{01296}* (Spradling et al., 1999), *tub-Gal4/TM3* (Lee and Luo, 1999), and *P[lacW]^{s1921}* (Spradling et al., 1999) were obtained from the Bloomington *Drosophila* Stock Center.

nero mutants were generated through imprecise excision of *P[lArB]^{K48}* and *P[lacW]^{s1921}*. *nero$^{k48\text{-}123}$* was generated from *P[lArB]^{K48}*. *nero^1* and *nero^2* alleles were generated from the mobilization of *P[lacW]^{s1921}*. Genomic lesions in *nero^1* and *nero^2* mutants were determined using PCR. *eIF5A^{Prev}* was generated through the excision of *P[PZ]^{01296}*.

Transgenic flies

To make a genomic rescue construct for *nero*, *Drosophila* genomic sequences corresponding to the *nero* locus were isolated from the DS00235 P1 clone (Berkeley *Drosophila* Genome Project). The P1 clone was digested with SacI, and this fragment was subcloned into the SacI site of the pBluescript cloning vector (Agilent Technologies). A 1.5-kb fragment was recovered from this construct by digesting with SwaI and MluI and was subcloned into the HpaI site of *P[CaSper4]*. To make *UAS-nero*, the CG2245 coding region was isolated from LD09536 (Berkeley *Drosophila* Genome Project *Drosophila* Gene Collection) and cloned into the EcoRI and XhoI sites of the *P[UAST]* vector. To make *UAS-eIF5A*, the CG3186 coding region was PCR amplified from RE47768 (Berkeley *Drosophila* Genome Project *Drosophila* Gold Collection) with adapters bearing EcoRI and XhoI sites and cloned into these sites of the *P[UAST]* vector. To make UAS-hDOHH and its enzymatically inactive versions, human cDNA (National Institutes of Health Mammalian Gene Collection) for DOHH was obtained from Invitrogen, PCR amplified, and cloned in pBluescript. H56A, H89A, H208A, and H240A point mutations in hDOHH were generated using a GeneTailor Site-Directed Mutagenesis system (Invitrogen). The wild-type and mutant versions were subsequently cloned into *P[UAST]*. All of these constructs were subsequently introduced into flies.

Antibody generation, Western blotting, immunohistochemistry, and BrdU assay

A full-length Nero–His tag fusion protein was generated by cloning the full-length Nero cDNA into the EcoRI and XhoI sites of the pET28a cloning vector (EMD). Coding sequences were amplified from LD09536 using primers that introduced EcoRI and XhoI restriction sites. The protein was induced in BL21 DE3 bacteria using IPTG and purified using His-Bind resin (EMD). Purified fusion proteins were injected into guinea pigs for antibody production (Cocalico Biologicals, Inc.).

We used standard protocols for Western blotting. Western Lightning Western Blot Chemiluminescence Reagent (PerkinElmer) was used to detect signal. Western blots were incubated in primary antibody using the following dilutions: 1:2,000 guinea pig anti–Nero GP25, 1:1,500 rabbit anti-eIF5A [EP526Y] (Abcam), and 1:10,000 mouse anti–actin C4 (MP Biomedicals).

For immunohistochemistry, larvae were dissected in PBS and fixed for 20 min in 4% formaldehyde in PBS. Standard protocols were used to label larval tissues with antibodies. Incubations in primary antibodies were performed overnight using the following dilutions: 1:100 mouse anti–Dlg 4F3 (Developmental Studies Hybridoma Bank), 1:400 rabbit anti-eIF5A [EP526Y] (Abcam), 1:400 mouse anti-KDEL (Assay Designs), 1:1,000 guinea pig anti–Nero GP26, and 1:2,000 rat anti-Su(H) (provided by F. Schweisguth, Institut Pasteur, Paris, France; Gho et al., 1996). Fluorescent Cy3- and Alexa Fluor 488–conjugated secondary antibodies (provided by

Jackson ImmunoResearch Laboratories and Invitrogen, respectively) were applied for 2 h at 1:200.

BrdU incorporation was conducted as previously described (Lee et al., 2005). However, discs were fixed in 4% formaldehyde for 1 h. 1:200 mouse anti–BrdU G3G4 (Developmental Studies Hybridoma Bank) was used to detect BrdU (Sigma-Aldrich) followed by subsequent detection with a fluorescent secondary antibody as described in the previous paragraph.

Autophagy assay

Autophagy assays were conducted as previously described (Scott et al., 2004). Larvae were dissected and incubated for 10 min in a 1:1,000 dilution of LysoTracker red DND-99 (Invitrogen) in PBS with DAPI to a final concentration of 0.4 µg/ml. LysoTracker was replaced with PBS before mounting and visualization.

Cell counting experiments

Newly hatched larvae were collected and placed in vials with standard food and allowed to develop at a density of 100 larvae per vial. 48 h after being selected, larvae were heat shocked at 37°C for 15 min. Larvae were allowed to develop to third instars and then dissected and fixed in 4% formaldehyde for 20 min. Dissected discs were treated with 400 µg/ml RNase A in PBS for 30 min at 37°C and then stained with propidium iodide (Invitrogen) at 1 µg/ml for 20 min before mounting.

Cell culture, RNAi, and polysome profile analysis

dsRNAs to *eIF5A*, *nero*, and *EGFP* were generated using a T7 RiboMAX Express RNAi system (Promega). Cells were treated as previously described (Clemens et al., 2000). 5×10^7 S2 cells were incubated with 100 µg/ml cycloheximide for 10 min, washed twice with cold PBS + 100 µg/ml cycloheximide, resuspended in lysis buffer (10 mM Hepes-KOH, pH 7.4, 5 mM $MgCl_2$, 150 mM KCl, 0.5% NP-40, 0.5 mM DTT, 100 µg/ml cycloheximide, 100 U/ml RNase inhibitor [Promega], and protease inhibitor [Roche]), homogenized with 10 strokes in a 3-ml dounce tissue grinder (Wheaton) on ice, and then centrifuged for 10 min at 14,000 *g*. The supernatants were loaded onto 10–50% sucrose gradients, which were prepared in 10 mM Hepes-KOH, pH 7.4, 5 mM $MgCl_2$, and 150 mM KCl, and centrifuged in a rotor (SW40; Beckman Coulter) at 35,000 rpm for 2 h. Gradients were analyzed by piercing the tube with a tube piercer (Brandel), passing 60% sucrose through the bottom of the tube using a syringe pump (Brandel) at a constant flow rate (0.75 ml/min), and monitoring the absorbance of the material eluting from the tube using a UV detector (UA-6; ISCO, Inc.) as previously described (Costa-Mattioli et al., 2005, 2007).

Microscopy

Samples were mounted in Vectashield mounting medium (Vector Laboratories) for confocal imaging. Confocal images were acquired using a confocal microscope (LSM510; Carl Zeiss, Inc.) with its accompanying software using Plan-Apochromat 40× NA 1.4 and Plan-Apochromat 63× NA 1.4 objectives (Carl Zeiss, Inc.). Images of fly adult thoraces (treated by boiling in 10% KOH) mounted in 70% glycerol were obtained using an LSM510 confocal microscope, camera (AxioCam HRc; Carl Zeiss, Inc.), Plan-Apochromat 10× NA 0.45 objective, and AxioVision 3.1 software (Carl Zeiss, Inc.). Images of fly eyes were captured with a camera (MicroFire; Olympus) mounted to a stereomicroscope (MZ16; Leica) using ImagePro Plus 5.0 acquisition software (Media Cybernetics). Fat bodies mounted in PBS for autophagy analysis were visualized using a microscope (Imager.Z1; Carl Zeiss, Inc.), camera (AxioCam MRm; Carl Zeiss, Inc.), AxioVision release 4.3 software (Carl Zeiss, Inc.), and either the Plan-Apochromat 10× NA 0.45 lens or the Plan-Apochromat 20× NA 0.75 lens. All images were later processed using ImageJ (National Institutes of Health) and Photoshop 7.0 (Adobe). All images were captured at room temperature.

Online supplemental material

Fig. S1 shows that no clear epistatic relationship can be established between *nero* and the Tor pathway. Online supplemental material is available at http://www.jcb.org/cgi/content/full/jcb.200904161/DC1.

We thank Koen Norga for plasmid rescue. We are grateful to T.F. MacKay, T.P. Neufeld, G. Struhl, G. Halder, P.H. Patel, F. Tamanoi, and the Bloomington *Drosophila* Stock Center for fly stocks. We are also grateful to F. Schweisguth and the Developmental Studies Hybridoma Bank for providing antibodies. We would also like to thank H. Pan and Y. He for technical assistance.

Confocal microscopy was supported by the Baylor College of Medicine Intellectual and Developmental Disabilities Research Center. This publication was made possible by a grant from the National Institute of Environmental Health Sciences, National Institutes of Health (T32 ES07332) to P.H. Patel. H.J. Bellen is a Howard Hughes Medical Institute Investigator.

Submitted: 30 April 2009
Accepted: 28 May 2009

Note added in proof. After this manuscript was accepted for publication, a paper appeared in *Nature* online (Saini et al. 2009. *Nature*. doi:10.1038/nature08034) showing that the depletion or inactivation of eIF5A in yeast (*S. cerevisiae*) results in the accumulation of polysomes, indicating that eIF5A promotes translation elongation. These data are in agreement with our observation that RNAi-mediated knockdown of either Nero or eIF5A blocks translation elongation and thus increases the size of polysomes in *Drosophila* S2 cells.

References

Abbruzzese, A., M.H. Park, and J.E. Folk. 1986. Deoxyhypusine hydroxylase from rat testis. Partial purification and characterization. *J. Biol. Chem.* 261:3085–3089.

Audibert, A., F. Simon, and M. Gho. 2005. Cell cycle diversity involves differential regulation of Cyclin E activity in the *Drosophila* bristle cell lineage. *Development*. 132:2287–2297.

Brand, A.H., and N. Perrimon. 1993. Targeted gene expression as a means of altering cell fates and generating dominant phenotypes. *Development*. 118:401–415.

Byers, T.L., J.R. Lakanen, J.K. Coward, and A.E. Pegg. 1994. The role of hypusine depletion in cytostasis induced by S-adenosyl-L-methionine decarboxylase inhibition: new evidence provided by 1-methylspermidine and 1,12-dimethylspermine. *Biochem. J.* 303:363–368.

Chatterjee, I., S.R. Gross, T.G. Kinzy, and K.Y. Chen. 2006. Rapid depletion of mutant eukaryotic initiation factor 5A at restrictive temperature reveals connections to actin cytoskeleton and cell cycle progression. *Mol. Genet. Genomics*. 275:264–276.

Chattopadhyay, M.K., C.W. Tabor, and H. Tabor. 2003. Spermidine but not spermine is essential for hypusine biosynthesis and growth in *Saccharomyces cerevisiae*: spermine is converted to spermidine in vivo by the FMS1-amine oxidase. *Proc. Natl. Acad. Sci. USA*. 100:13869–13874.

Clemens, J.C., C.A. Worby, N. Simonson-Leff, M. Muda, T. Maehama, B.A. Hemmings, and J.E. Dixon. 2000. Use of double stranded RNA interference in *Drosophila* cell lines to dissect signal transduction pathways. *Proc. Natl. Acad. Sci. USA*. 97:6499–6503.

Cooper, H.L., M.H. Park, J.E. Folk, B. Safer, and R. Braverman. 1983. Identification of the hypusine-containing protein hy+ as translation initiation factor eIF-4D. *Proc. Natl. Acad. Sci. USA*. 80:1854–1857.

Costa-Mattioli, M., D. Gobert, H. Harding, B. Herdy, M. Azzi, M. Bruno, M. Bidinosti, C. Ben Mamou, E. Marcinkiewicz, M. Yoshida, et al. 2005. Translational control of hippocampal synaptic plasticity and memory by the eIF2alpha kinase GCN2. *Nature*. 436:1166–1173.

Costa-Mattioli, M., D. Gobert, E. Stern, K. Gamache, R. Colina, C. Cuello, W. Sossin, R. Kaufman, J. Pelletier, K. Rosenblum, et al. 2007. eIF2alpha phosphorylation bidirectionally regulates the switch from short- to long-term synaptic plasticity and memory. *Cell*. 129:195–206.

Dann, S.G., and G. Thomas. 2006. The amino acid sensitive TOR pathway from yeast to mammals. *FEBS Lett.* 580:2821–2829.

Dietzl, G., D. Chen, F. Schnorrer, K.C. Su, Y. Barinova, M. Fellner, B. Gasser, K. Kinsey, S. Oppel, S. Scheiblauer, et al. 2007. A genome-wide transgenic RNAi library for conditional gene inactivation in *Drosophila*. *Nature*. 448:151–156.

Fischer, J.A., E. Giniger, T. Maniatis, and M. Ptashne. 1988. GAL4 activates transcription in *Drosophila*. *Nature*. 332:853–856.

Gao, X., and D. Pan. 2001. TSC1 and TSC2 tumor suppressors antagonize insulin signaling in cell growth. *Genes Dev.* 15:1383–1392.

Garcia-Bellido, A., and J.R. Merriam. 1971. Genetic analysis of cell heredity in imaginal discs of *Drosophila melanogaster*. *Proc. Natl. Acad. Sci. USA*. 68:2222–2226.

Gho, M., M. Lecourtois, G. Geraud, J.W. Posakony, and F. Schweisguth. 1996. Subcellular localization of Suppressor of Hairless in *Drosophila* sense organ cells during Notch signalling. *Development*. 122:1673–1682.

Gordon, E.D., R. Mora, S.C. Meredith, C. Lee, and S.L. Lindquist. 1987. Eukaryotic initiation factor 4D, the hypusine-containing protein, is conserved amongst eukaryotes. *J. Biol. Chem.* 262:16585–16589.

Gratzner, H.G. 1982. Monoclonal antibody to 5-bromo- and 5-iododeoxyuridine: a new reagent for detection of DNA replication. *Science*. 218:474–475.

Gregio, A.P., V.P. Cano, J.S. Avaca, S.R. Valentini, and C.F. Zanelli. 2009. eIF5A has a function in the elongation step of translation in yeast. *Biochem. Biophys. Res. Commun.* 380:785–790.

Hanauske-Abel, H.M., M.H. Park, A.R. Hanauske, A.M. Popowicz, M. Lalande, and J.E. Folk. 1994. Inhibition of the G1-S transition of the cell cycle by inhibitors of deoxyhypusine hydroxylation. *Biochim. Biophys. Acta*. 1221:115–124.

Jakus, J., E.C. Wolff, M.H. Park, and J.E. Folk. 1993. Features of the spermidine-binding site of deoxyhypusine synthase as derived from inhibition studies. Effective inhibition by bis- and mono-guanylated diamines and polyamines. *J. Biol. Chem.* 268:13151–13159.

Joe, Y.A., E.C. Wolff, and M.H. Park. 1995. Cloning and expression of human deoxyhypusine synthase cDNA. Structure-function studies with the recombinant enzyme and mutant proteins. *J. Biol. Chem.* 270:22386–22392.

Kang, H.A., and J.W. Hershey. 1994. Effect of initiation factor eIF-5A depletion on protein synthesis and proliferation of *Saccharomyces cerevisiae*. *J. Biol. Chem.* 269:3934–3940.

Kang, K.R., E.C. Wolff, M.H. Park, J.E. Folk, and S.I. Chung. 1995. Identification of YHR068w in *Saccharomyces cerevisiae* chromosome VIII as a gene for deoxyhypusine synthase. Expression and characterization of the enzyme. *J. Biol. Chem.* 270:18408–18412.

Kang, K.R., Y.S. Kim, E.C. Wolff, and M.H. Park. 2007. Specificity of the deoxyhypusine hydroxylase-eukaryotic translation initiation factor (eIF5A) interaction: identification of amino acid residues of the enzyme required for binding of its substrate, deoxyhypusine-containing eIF5A. *J. Biol. Chem.* 282:8300–8308.

Kim, Y.S., K.R. Kang, E.C. Wolff, J.K. Bell, P. McPhie, and M.H. Park. 2006. Deoxyhypusine hydroxylase is a Fe(II)-dependent, HEAT-repeat enzyme. Identification of amino acid residues critical for Fe(II) binding and catalysis. *J. Biol. Chem.* 281:13217–13225.

Lee, S.B., J. Park, J.U. Jung, and J. Chung. 2005. Nef induces apoptosis by activating JNK signaling pathway and inhibits NF-kappaB-dependent immune responses in *Drosophila*. *J. Cell Sci.* 118:1851–1859.

Lee, T., and L. Luo. 1999. Mosaic analysis with a repressible cell marker for studies of gene function in neuronal morphogenesis. *Neuron*. 22:451–461.

Lyman, R.F., F. Lawrence, S.V. Nuzhdin, and T.F. Mackay. 1996. Effects of single P-element insertions on bristle number and viability in *Drosophila melanogaster*. *Genetics*. 143:277–292.

Moreno, E., K. Basler, and G. Morata. 2002. Cells compete for decapentaplegic survival factor to prevent apoptosis in *Drosophila* wing development. *Nature*. 416:755–759.

Neufeld, T.P., A.F. de la Cruz, L.A. Johnston, and B.A. Edgar. 1998. Coordination of growth and cell division in the *Drosophila* wing. *Cell*. 93:1183–1193.

Norga, K.K., M.C. Gurganus, C.L. Dilda, A. Yamamoto, R.F. Lyman, P.H. Patel, G.M. Rubin, R.A. Hoskins, T.F. Mackay, and H.J. Bellen. 2003. Quantitative analysis of bristle number in *Drosophila* mutants identifies genes involved in neural development. *Curr. Biol.* 13:1388–1396.

Oldham, S., J. Montagne, T. Radimerski, G. Thomas, and E. Hafen. 2000. Genetic and biochemical characterization of dTOR, the *Drosophila* homolog of the target of rapamycin. *Genes Dev.* 14:2689–2694.

Park, M.H., H.L. Cooper, and J.E. Folk. 1982. The biosynthesis of protein-bound hypusine (N epsilon -(4-amino-2-hydroxybutyl)lysine). Lysine as the amino acid precursor and the intermediate role of deoxyhypusine (N epsilon -(4-aminobutyl)lysine). *J. Biol. Chem.* 257:7217–7222.

Park, M.H., E.C. Wolff, Y.B. Lee, and J.E. Folk. 1994. Antiproliferative effects of inhibitors of deoxyhypusine synthase. Inhibition of growth of Chinese hamster ovary cells by guanyl diamines. *J. Biol. Chem.* 269:27827–27832.

Park, M.H., Y.B. Lee, and Y.A. Joe. 1997. Hypusine is essential for eukaryotic cell proliferation. *Biol. Signals*. 6:115–123.

Park, M.H., Y.A. Joe, and K.R. Kang. 1998. Deoxyhypusine synthase activity is essential for cell viability in the yeast *Saccharomyces cerevisiae*. *J. Biol. Chem.* 273:1677–1683.

Park, J.H., E.C. Wolff, J.E. Folk, and M.H. Park. 2003. Reversal of the deoxyhypusine synthesis reaction. Generation of spermidine or homospermidine from deoxyhypusine by deoxyhypusine synthase. *J. Biol. Chem.* 278:32683–32691.

Park, J.H., L. Aravind, E.C. Wolff, J. Kaevel, Y.S. Kim, and M.H. Park. 2006. Molecular cloning, expression, and structural prediction of deoxyhypusine hydroxylase: a HEAT-repeat-containing metalloenzyme. *Proc. Natl. Acad. Sci. USA*. 103:51–56.

Pelham, H.R. 1990. The retention signal for soluble proteins of the endoplasmic reticulum. *Trends Biochem. Sci.* 15:483–486.

Pi, H., H.J. Wu, and C.T. Chien. 2001. A dual function of phyllopod in *Drosophila* external sensory organ development: cell fate specification of sensory organ precursor and its progeny. *Development*. 128:2699–2710.

Potter, C.J., H. Huang, and T. Xu. 2001. *Drosophila* Tsc1 functions with Tsc2 to antagonize insulin signaling in regulating cell growth, cell proliferation, and organ size. *Cell*. 105:357–368.

Rusten, T.E., K. Lindmo, G. Juhasz, M. Sass, P.O. Seglen, A. Brech, and H. Stenmark. 2004. Programmed autophagy in the *Drosophila* fat body is induced by ecdysone through regulation of the PI3K pathway. *Dev. Cell*. 7:179–192.

Sasaki, K., M.R. Abid, and M. Miyazaki. 1996. Deoxyhypusine synthase gene is essential for cell viability in the yeast *Saccharomyces cerevisiae*. *FEBS Lett.* 384:151–154.

Schnier, J., H.G. Schwelberger, Z. Smit-McBride, H.A. Kang, and J.W. Hershey. 1991. Translation initiation factor 5A and its hypusine modification are essential for cell viability in the yeast *Saccharomyces cerevisiae*. *Mol. Cell. Biol.* 11:3105–3114.

Scott, R.C., O. Schuldiner, and T.P. Neufeld. 2004. Role and regulation of starvation-induced autophagy in the *Drosophila* fat body. *Dev. Cell*. 7:167–178.

Smit-McBride, Z., T.E. Dever, J.W. Hershey, and W.C. Merrick. 1989. Sequence determination and cDNA cloning of eukaryotic initiation factor 4D, the hypusine-containing protein. *J. Biol. Chem.* 264:1578–1583.

Spradling, A.C., D. Stern, A. Beaton, E.J. Rhem, T. Laverty, N. Mozden, S. Misra, and G.M. Rubin. 1999. The Berkeley *Drosophila* Genome Project gene disruption project: Single P-element insertions mutating 25% of vital *Drosophila* genes. *Genetics*. 153:135–177.

Tapon, N., N. Ito, B.J. Dickson, J.E. Treisman, and I.K. Hariharan. 2001. The *Drosophila* tuberous sclerosis complex gene homologs restrict cell growth and cell proliferation. *Cell*. 105:345–355.

Wöhl, T., H. Klier, H. Ammer, F. Lottspeich, and V. Magdolen. 1993. The HYP2 gene of *Saccharomyces cerevisiae* is essential for aerobic growth: characterization of different isoforms of the hypusine-containing protein Hyp2p and analysis of gene disruption mutants. *Mol. Gen. Genet.* 241:305–311.

Wolff, E.C., M.H. Park, and J.E. Folk. 1990. Cleavage of spermidine as the first step in deoxyhypusine synthesis. The role of NAD. *J. Biol. Chem.* 265:4793–4799.

Woods, D.F., and P.J. Bryant. 1991. The discs-large tumor suppressor gene of *Drosophila* encodes a guanylate kinase homolog localized at septate junctions. *Cell*. 66:451–464.

Xu, T., and G.M. Rubin. 1993. Analysis of genetic mosaics in developing and adult *Drosophila* tissues. *Development*. 117:1223–1237.

Zanelli, C.F., A.L. Maragno, A.P. Gregio, S. Komili, J.R. Pandolfi, C.A. Mestriner, W.R. Lustri, and S.R. Valentini. 2006. eIF5A binds to translational machinery components and affects translation in yeast. *Biochem. Biophys. Res. Commun.* 348:1358–1366.

Zhang, H., J.P. Stallock, J.C. Ng, C. Reinhard, and T.P. Neufeld. 2000. Regulation of cellular growth by the *Drosophila* target of rapamycin dTOR. *Genes Dev.* 14:2712–2724.